



Controlling donor and newborn neuron migration and maturation in the eye through microenvironment engineering

Jonathan R. Soucy^{a,b} , Levi Todd^c , Emil Kriukov^{a,b}, Monichan Phay^{a,b}, Volha V. Malechka^{a,b}, John Dayron Rivera^{a,b}, Thomas A. Reh^c, and Petr Baranov^{a,b,1}

Edited by Carol Mason, Columbia University, New York, NY; received February 7, 2023; accepted September 30, 2023

Ongoing cell therapy trials have demonstrated the need for precision control of donor cell behavior within the recipient tissue. We present a methodology to guide stem cell-derived and endogenously regenerated neurons by engineering the microenvironment. Being an “approachable part of the brain,” the eye provides a unique opportunity to study neuron fate and function within the central nervous system. Here, we focused on retinal ganglion cells (RGCs)—the neurons in the retina are irreversibly lost in glaucoma and other optic neuropathies but can potentially be replaced through transplantation or reprogramming. One of the significant barriers to successful RGC integration into the existing mature retinal circuitry is cell migration toward their natural position in the retina. Our *in silico* analysis of the single-cell transcriptome of the developing human retina identified six receptor-ligand candidates, which were tested in functional *in vitro* assays for their ability to guide human stem cell-derived RGCs. We used our lead molecule, SDF1, to engineer an artificial gradient in the retina, which led to a 2.7-fold increase in donor RGC migration into the ganglion cell layer (GCL) and a 3.3-fold increase in the displacement of newborn RGCs out of the inner nuclear layer. Only donor RGCs that migrated into the GCL were found to express mature RGC markers, indicating the importance of proper structure integration. Together, these results describe an “*in silico*–*in vitro*–*in vivo*” framework for identifying, selecting, and applying soluble ligands to control donor cell function after transplantation.

retinal organoids | glaucoma | transplantation | stem cells | chemokines

Approximately 3.5% of the world’s population over 40 has glaucoma, the most common optic neuropathy (1). By 2040, the global prevalence of glaucoma will exceed 110 million people as the population ages (2), making it a high-priority target for therapy development. Although several neuroprotective approaches focused on preserving existing cells and their axons are being explored (3, 4), this strategy alone will not restore vision already lost due to cell death. The mammalian retina has a limited capacity to regenerate; thus, retinal neuron death leads to irreversible vision loss (5). Retinal ganglion cell (RGC) replacement is needed to recover sight loss to glaucoma.

RGC replacement remains an unsolved challenge in regenerative ophthalmology. Success would help bring vision back to millions of advanced-state glaucoma patients. Recent advancements enable transplantation of primary rodent RGCs (6–8), differentiation of RGCs from human pluripotent stem cells (9, 10), reprogramming Müller glia to RGCs (11), and functional axon regeneration to the brain suggest that transplantation-mediated vision repair may be feasible (12).

We demonstrated the robust survival of induced pluripotent stem cell (iPSC)-derived RGCs following intravitreal transplantation into healthy and damaged retinas (13). These studies became possible due to robust RGC differentiation and isolation from iPSC cultures established in our lab (14–16). Despite those successes, the survival rate for individual RGCs remains low, and most donor neurons remain above the inner limiting membrane that defines the neural retinal border with the vitreous cavity without integrating (17). The highly conserved organization of the retina across species suggests a relationship between retinal structure and function (18). This challenge is not unique to RGC replacement. Poor structural integration is a significant obstacle to neuron transplantation (e.g., photoreceptors, dopaminergic, and motor neurons) and transdifferentiation (e.g., glia to cerebral and retinal neurons) (11, 19). There are nonsurgical techniques for inner limiting membrane disruption and removal of this existing anatomical barrier (20, 21); however, integration critically depends on the modulation of the host’s adult retinal environment, and inner limiting membrane disruption may not be appropriate in a clinical setting (22).

Significance

The “*in silico*–*in vitro*–*in vivo*” funnel holds significant potential for identifying targets to control cellular processes in research and clinical applications. In this report, we describe a framework for identifying, selecting, and applying chemokines to direct retinal neuron migration *in vivo* within the adult mouse retina. To reach a broader audience, we demonstrate this phenomenon using dissociated mouse and human stem cell-derived retinal neurons, retinal organoids, and endogenously reprogrammed retinal neurons. Last, we show that only neurons that migrate into their proper lamina after transplantation express mature cell markers, indicating the importance of driving structural integration for neuron transplantation.

Author contributions: J.R.S. and P.B. designed research; J.R.S., L.T., M.P., V.V.M., J.D.R., T.A.R., and P.B. performed research; J.R.S. and M.P. contributed new reagents/analytic tools; J.R.S. and E.K. analyzed data; and J.R.S. wrote the paper.

Competing interest statement: The University of Washington has a patent incorporating the endogenous reprogramming technology described in this report with inventors L.T. and T.A.R.

This article is a PNAS Direct Submission.

Copyright © 2023 the Author(s). Published by PNAS. This open access article is distributed under [Creative Commons Attribution-NonCommercial-NoDerivatives License 4.0 \(CC BY-NC-ND\)](https://creativecommons.org/licenses/by-nc-nd/4.0/).

¹To whom correspondence may be addressed. Email: petr_baranov@meei.harvard.edu.

This article contains supporting information online at <https://www.pnas.org/lookup/suppl/doi:10.1073/pnas.2302089120/-DCSupplemental>.

Published November 6, 2023.

We hypothesize that early guided migration can significantly improve the structural and functional integration of donor and newborn RGCs.

Neurogenesis in the mammalian retina completes shortly after birth (23–25). Thus, the transplantation of stem cells and their progeny relies on the recapitulation of the development and/or regenerative pathways. During development, RGCs, like most early-born neurons, migrate via somal translocation, but confocal traces in zebrafish demonstrate that RGCs migrate through multipolar migration if somal translocation is inhibited (26). Multipolar migration does not rely on the extension and attachment of neural processes to reach their final location and is the preferred migratory mode for late-born neurons that navigate through developed tissues (27, 28). It is unknown whether RGCs are capable of multipolar migration in mammals, and the exact mechanism by which stem cell-derived donor RGCs migrate within the mature retina remains unknown. It is also unclear whether newborn and stem cell-derived RGCs can respond to chemokines, previously identified in the studies of retinal and cerebral development and neuron migration in the brain out of the subventricular zone during postnatal regeneration (29).

Here, we describe a framework to identify, select, and apply chemokines to direct cell migration *in vivo* within the retina. We performed an *in silico* analysis of the single-cell transcriptome of developing human retinas and identified six receptor-ligand candidates to guide stem cell-derived or newborn neurons. The lead candidates were then tested in the functional *in vitro* assays for their ability to guide stem cell-derived RGCs, with stromal cell-derived factor-1 (SDF1) identified as the most potent chemokine for RGC recruitment. For this and other experiments, we differentiated RGCs from mouse and human stem cells using retinal organoid cultures or stimulated glial reprogramming to neurons with proneuronal transcription factors (11, 30, 31). We then transplanted these stem cell-derived RGCs subretinally and delivered recombinant SDF1 protein intravitreally to establish a chemokine gradient across the retina. Using a quantitative approach to transplantation, we confirmed that donor cell behavior is controllable by modulating the tissue microenvironment. Furthermore, we demonstrate that an SDF1 gradient across the host retina enhances the structural integration of mouse and human stem cell-derived donor RGCs via multipolar migration. Interestingly, only RGCs that successfully integrated into the ganglion cell layer (GCL) were shown to express RNA-binding protein with multiple splicing (RBPM5), a mature RGC marker. Last, we demonstrate that intravitreal delivery of SDF1 increases the displacement of newborn RGCs out of the inner nuclear layer and toward their natural connecting points in the retina. Altogether, this is a demonstration of the universal nature and applicability of neurokinin-directed controlled migration of donor stem cell-derived and endogenously regenerated neurons. Moreover, the established workflow to identify microenvironment modifiers can be ported to control other aspects of donor neuron behavior.

Results and Discussion

Donor Stem Cell-Derived RGCs Fail to Migrate into the Retina Spontaneously. We and others have demonstrated the feasibility of cell replacement therapy with RGCs isolated from the developing retina and stem cell-derived RGCs. Our grafts survived in healthy and damaged retinas following xeno- and allo-transplantation and sent projections into the optic nerve (13). Cell survival does not equal functional integration; therefore, better structural integration is needed to achieve vision restoration. While more than 60% of recipients have donor RGCs at 2 wk to 1 y in our syngeneic transplantation study (13), the proportion of surviving

cells typically remains low (<5%), and even fewer cells migrate completely into the GCL (<1%). Recently, Zhang et al. showed that stem cell-derived human RGCs cultured on the neuroretina explant could not migrate through the inner limiting membrane to graft into the GCL, and disruption of this barrier resulted in increased structural integration (20). However, while it is possible to degrade or surgically remove the inner limiting membrane, these procedures pose a significant risk of damaging the retina (22). Moreover, the inner limiting membrane has been shown to play an essential role in the proper lamination of the retina (32). Therefore, we sought to explore subretinal delivery as an alternative approach for transplanting donor neurons while leaving the inner limiting membrane completely intact.

Subretinal delivery has proven an effective strategy for gene, photoreceptor, and retinal pigment epithelium delivery. However, unlike these transplantation paradigms, where the cells are delivered directly to their final position, RGCs must migrate more than 200 μm into the GCL. While our previous work suggests that the subretinal space supports donor RGC survival, we did not observe any migration toward the GCL using this approach (13). During development, RGCs are born on the apical surface and migrate toward the basal side into what will become the GCL, but we do not yet know whether this is due to an intrinsic RGC capacity or a response to the developmental retinal microenvironment. To investigate this phenomenon, we delivered mouse stem cell-derived RGCs using intravitreal and subretinal approaches to study the positions of the donor cells within the neural retina. Two weeks posttransplantation, mice were euthanized according to the Schepens Eye Research Institute Institutional Animal Care and Use Committee guidelines, and retinas were stained and mounted to access donor RGC distribution (Fig. 1A). We observed no spontaneous migration through the inner limiting membrane for RGCs delivered intravitreally (Fig. 1B) but demonstrated limited migration through the neural retina for RGCs delivered subretinally (Fig. 1C). Despite having a limited capacity for spontaneous migration following subretinal cell delivery and very few RGCs integrating into the GCL, these results suggest that the subretinal delivery route is a viable alternative to intravitreal delivery so that RGCs can circumvent the inner limiting membrane. Moreover, because spontaneous migration only occurred by mimicking development with our subretinal delivery approach, we hypothesize that neuron migration in the retina must be driven by a response to the developmental microenvironment.

Identifying Migration Cues through Single-cell RNA Sequencing Analysis of the Developing and Adult Human Retina. To investigate RGC migration in the developing retina, we sourced available human fetal and adult retina single-cell RNA sequencing data to explore which pro-migratory signals are up-regulated during RGC development (33, 34). There are two major neuron migration patterns in retinal and cerebral development: radial and tangential (35). Tangential migration means that neurons follow the axis perpendicular to the tissue's apicobasal axis (XY plane), but this rarely occurs in the vertebrate retina (36), where most neurons and progenitors travel radially. RGCs are the first-born retinal neurons in the retina, and after their separation from the intermediate committed precursor, they migrate to the most basal layer adjacent to the lens (Z axis). Confocal tracing of individual RGCs shows that this happens through somal translocation during development (37). Somal translocation involves a neuron sending its process toward its final location and translocating its cell body along that process (38). A challenge in extrapolating these findings to cell transplantation in a developed eye is the lack of developmentally relevant chemokine gradient in the mature retina.

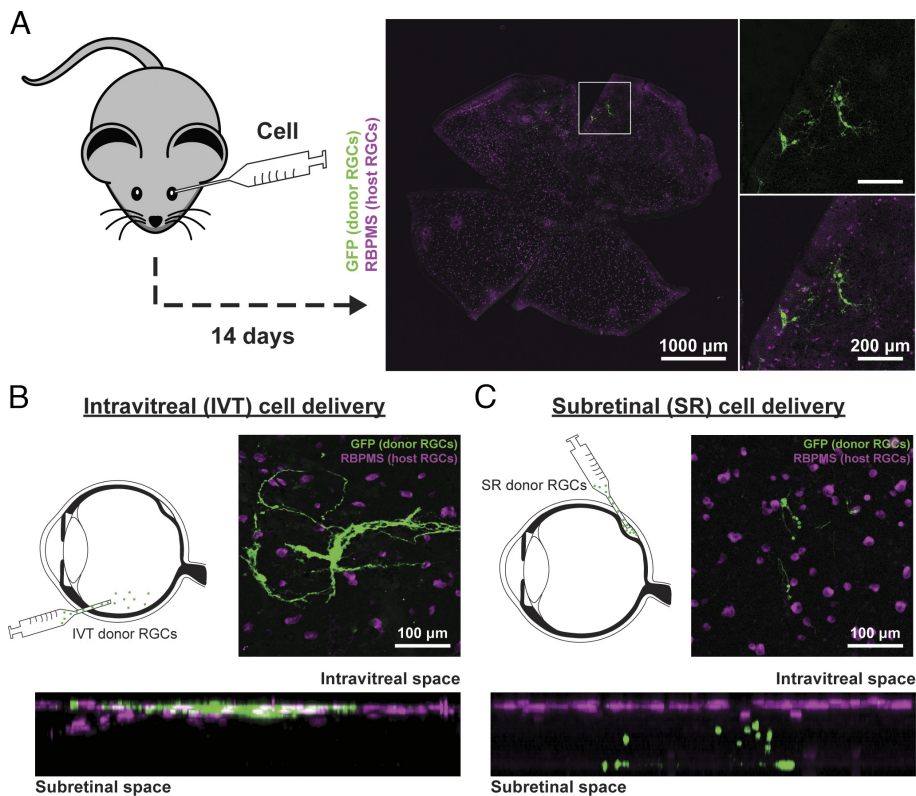


Fig. 1. Spontaneous RGC migration toward the GCL following subretinal delivery in mice. (A) Representative immunofluorescent image of a mouse retinal flat mount (max intensity projection) stained for host (RBPMS+) and donor (mThy1.2-GFP+) RGCs 14 d posttransplantation. (B) Representative max intensity projection and orthographic projection of a retinal flat mount following intravitreal delivery and (C) subretinal delivery of donor RGCs.

The regeneration and renewal of RGCs in lower vertebrates may be more relevant for the transplantation setting. In zebrafish, RGCs can move through multipolar migration with several processes extending from a cell (39); however, it is not known whether such a pattern exists in mammalian RGCs.

We performed cluster identification using published single-cell RNA sequencing data to define each retinal neuron population (Fig. 2 A–D). RGCs were then subclustered based on their expression of mature (RBPMS) and immature (POU4F2) markers (Fig. 2 A–D, feature plots). Interestingly, similar to an injury or disease model in mice where RGC transcription factors are down-regulated (40, 41), in human development, POU4F2 seems to be down-regulated with age. As a result, we do not yet know whether this downregulation is a consequence of damage during sample preparation or whether POU4F2 downregulation is a part of normal human RGC maturation. Nevertheless, we quantified the gene expression changes associated with multipolar migration and somal translocation and performed a gene set enrichment analysis (escape package) (42, 43) on RGCs under the assumption that POU4F2 and RBPMS represent different developmental stages. During early development, neuronal migration genes were more highly expressed, but as RGCs matured (FD82, RBPMS+), the expression of these genes decreased (Fig. 2E), indicating that RGC migration occurs early in development and primarily for immature RGCs. Further analysis revealed that genes corresponding to multipolar migration and somal translocation have different expression patterns, with multipolar migration genes having their highest expression later in development than somal translocation genes (Fig. 2F). These results are consistent with the fact that multipolar migration is the preferred migratory mode for late-born neurons that need to navigate through more complex tissue and cellular structures (27, 28). Therefore, the multipolar migration and somal translocation gene expression patterns shown here are indirect evidence of different modes of RGC migration within the human retina

during development. However, despite the evidence of host RGC migration, these data do not indicate how neuron migration is controlled in the retina.

The neuron migration can be mediated through transcription factors, adhesion molecules, ion channels, and extracellular cues/receptors (35). Here, we focused on pro-migratory receptors since these are the most amenable for modulation through engineering the microenvironment. We screened all the receptors associated with neuron migration that had higher expression in the POU4F2+ RGC vs. RBPMS+ RGC subclusters and identified six candidates from this in silico analysis to investigate further: adhesion G protein-coupled receptor G1 (ADGRG1), C-X-C motif chemokine receptor type 4 (CXCR4), deleted in colorectal cancer/netrin receptor DCC (DCC), frizzled class receptor 3 (FZD3), nuclear receptor subfamily 2 group F member 1 (NR2F1), and roundabout guidance receptor 2 (ROBO2) (Fig. 2G).

Based on this single-cell RNA sequencing analysis and previous cell migration studies (44), we selected a subset of these chemokine receptors to enhance and control neuron cell migration. From the identified receptors, ADGRG1 was excluded because it is a negative regulator of cell migration (45), FZD3 was excluded because its ligand, WNT is a key regulator of RGC differentiation (30), and NR2F1 was excluded because its ligand is currently unknown (46). Fibroblast growth factor receptor (FGFR) was added as a positive control based on prior studies (47, 48), and protein patched homolog 1 (PTCH1) was added because sonic hedgehog protein (SHH) is required for normal laminar organization in the vertebrate retina (49). We confirmed the expression of our panel of chemokine receptors in the developing retina and observed different expression levels in each neuron population at each time point (SI Appendix, Fig. S1).

CXCR4 Activation by SDF1 Enhances RGC Recruitment In Vitro. The human stem cell-derived RGCs were used to investigate our ability to control neuron migration. Human RGCs were differentiated from Brn3b-tdTomato hESC in organoid cultures

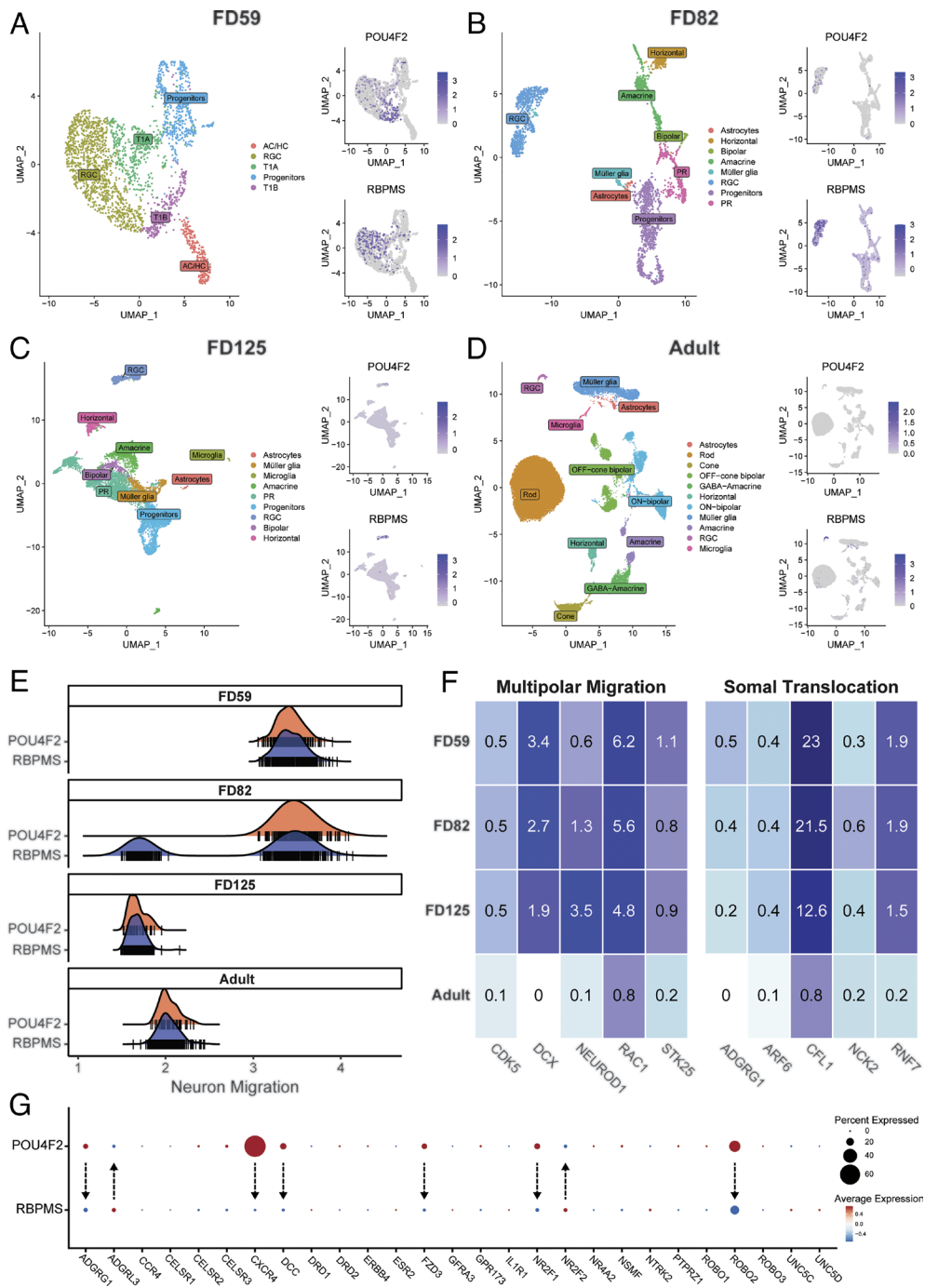


Fig. 2. Characterization of human RGC migration patterns and receptor expression during development. (A) Dimplot of the human neural retina with clusters identified by cell type-specific gene expression and feature plots showing characteristic genes describing clusters of mature (RBPMS) and immature (POU4F2) RGCs during fetal day 59, (B) fetal day 82, (C) fetal day 125, and (D) adulthood. (E) Gene set enrichment analysis of mature and immature RGC populations during different developmental ages shows the upregulation of genes associated with migration early in development and in immature RGCs. (F) Heat map comparison of the most highly expressed genes related to multipolar migration and somal translocation shows that somal translocation has the highest expression of these genes during early development (FD59), while multipolar migration has the highest expression of these genes in later stages of development (FD82–125) with little to no expression during adulthood. (G) Dot plot showing the percent and average expression in mature (RBPMS) and immature (POU4F2) RGCs for receptors known to be involved in neural migration. Each arrow shows a decrease in expression for all the receptors expressed in >5% of RGCs and helps to define which receptors may be critical for early RGC migration during development.

using a three dimensional-two dimensional-three dimensional (3D-2D-3D) technique to parallel development. By recapitulating development in 3D, we expect RGCs differentiated within retinal organoids to have a receptor expression and migratory potential similar to human RGCs (33).

During the first 3D phase, embryoid bodies are formed by forced aggregation, anterior neural development promoted by WNT inhibition, and retinal differentiation amplified by BMP4 signaling (Fig. 3A). Optic vesicles from the resulting organoid were dissected by random chopping and allowed to attach to a 2D surface to generate an epithelial cell layer (Fig. 3B). During this epithelial formation, retinal progenitor expansion was enhanced by sonic hedgehog activation. Retinal aggregates were then transitioned back to 3D culture and maintained in long-term retinal differentiation media (LT-RDM) that was later supplemented with all-trans retinoic acid

to increase the survival and differentiation of RGCs (Fig. 3A). RGCs were isolated from organoid cultures using enzymatic dissociation and magnetic bead sorting against CD90.2 after 42 to 50 d of differentiation. RGCs differentiated from Brn3b-*tdTomato* hESC were visualized by the expression of the *tdTomato* reporter (Fig. 3B). Finally, stem cell-derived RGCs were confirmed to express receptors for acidic fibroblast growth factor (aFGF), Netrin1, SHH, Slit1, and SDF1 (*SI Appendix*, Fig. S2A).

To identify our lead candidate for RGC recruitment, we studied the migration of human RGC in response to different chemokine gradients in vitro. Using a transwell assay, we evaluated the effect of aFGF, Netrin1, SHH, Slit1, and SDF1 on RGC recruitment (Fig. 3C). Chemokine concentrations were selected based on prior work, and a nontreated control was included as a negative control. RGCs were seeded on the apical surface of the membrane and migrated through

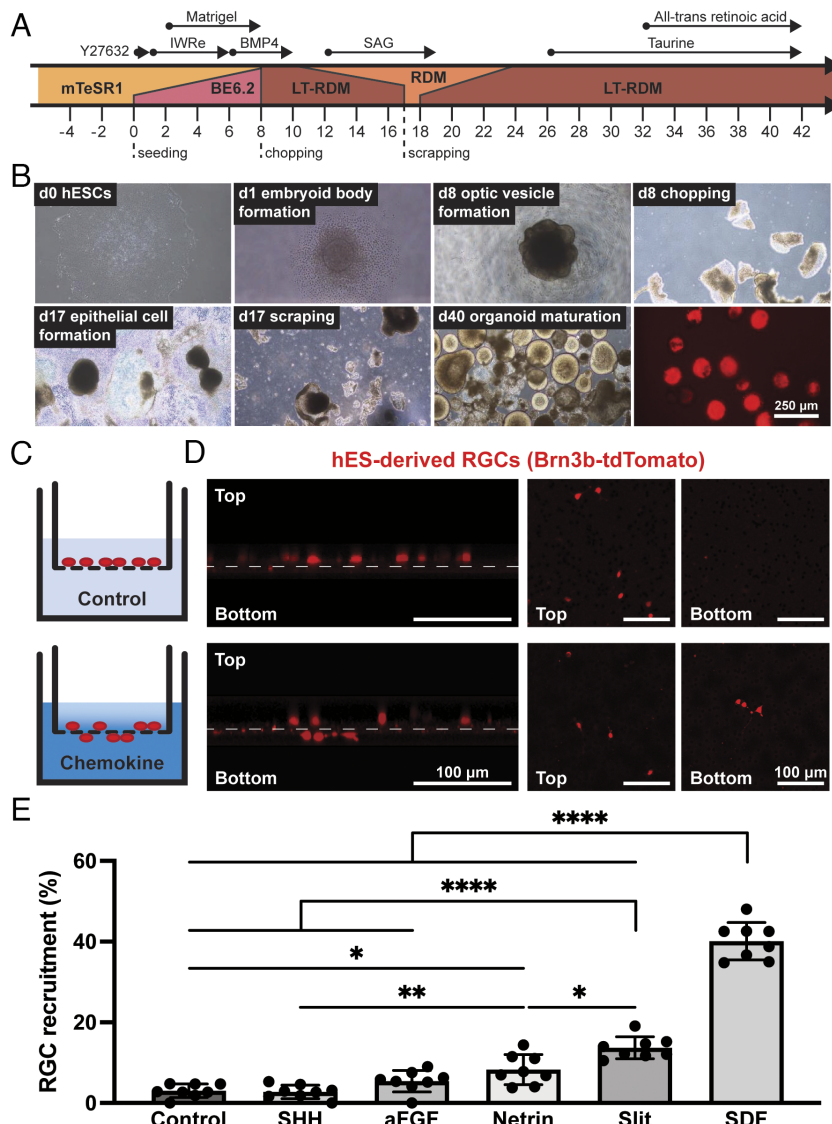


Fig. 3. Human stem cell-derived RGCs migrate in response to chemokines. (A) Schematic overview summarizing hESC differentiation into retinal organoids using a 3D-2D-3D technique adopted from the Meyer and Zack labs (30, 31). LT-RDM, long-term retinal differentiation media. (B) Representative images of important stages in RGC differentiation starting from hESCs to form embryoid bodies and optic vesicle-like structures in 3D culture before being moved to 2D culture to enable epithelial cell formation and then back to 3D culture to mature and generate RGCs (tdTomato positive cells). (C) Schematic of cell recruitment transwell assay and (D) representative immunofluorescent 3D reconstruction and en-face images of hRGCs on the apical and/or basal membrane surface following chemokine treatment. (E) Quantitative analysis of RGC recruitment, defined as the ratio of RGCs on the basal surface to the total number of RGCs, in response to 500 ng/mL SHH, 250 ng/mL aFGF, 100 ng/mL Netrin, 1,000 ng/mL Slit, and 50 ng/mL SDF1 treatment. N = 8 wells per group.

the pores (8 microns) over 24 h. RGCs were counted in the same areas on both sides of the membrane, and RGC recruitment was calculated as the ratio of cells on the basal surface to the total number of cells (Fig. 3D). Netrin1, Slit1, and SDF1 treatment significantly increased cell recruitment compared with the control, whereas aFGF and SHH showed no statistically significant differences compared to the non-treated control (Fig. 3E). SDF1 led to the most significant increase in RGC recruitment, with $40.11 \pm 4.62\%$ of RGCs migrating onto the basal membrane surface. Interestingly, despite being included as a positive control, aFGF failed to cause a significant increase in RGC recruitment, highlighting the power of our approach toward identifying targets to control neuron behavior.

After identifying SDF1 as the most potent chemokine for RGC recruitment, we sought to better characterize and understand this mechanism. To further validate CXCR4 expression in our RGCs, we performed an immunohistochemistry analysis on cultured RGCs. While CXCR4 seems to be expressed in all tdTomato-positive cells (*SI Appendix*, Fig. S2B), it is also expressed in tdTomato-negative cell populations (*SI Appendix*, Fig. S2C, yellow arrow). We confirmed this result by flow cytometry and single-cell RNA sequencing of retinal organoids. Flow cytometry shows that greater than 85% of all tdTomato-positive cells (hRGCs) express CXCR4 by flow cytometry (*SI Appendix*, Fig. S2D). Similarly, by single-cell RNA sequencing, we show that greater than 55% of the RGC cluster express CXCR4

(*SI Appendix*, Fig. S3). Interestingly, while most hRGCs express CXCR4, only ~40% migrated in response to SDF1 treatment. Therefore, we again adopted our transwell assay to evaluate the effect of SDF1 concentration on RGC recruitment to understand whether this response is dose-mediated. Using the same approach, we evaluated various concentrations of SDF1: 0, 10, 50, 200, and 500 ng/mL. When compared to the control, 10, 50, and 200 ng/mL SDF1 resulted in significantly enhanced RGC recruitment, but there was no statistically significant difference between 50 and 200 ng/mL SDF1 (*SI Appendix*, Fig. S4A, $39.71 \pm 5.67\%$ vs. $45.85 \pm 7.52\%$), indicating some upper limit to this dose-response. No RGCs remained attached to the membranes in cultures treated with 500 ng/mL SDF. We do not yet know whether there is a subset of nonmotile RGCs that represent a particular state of RGC maturation or whether different RGC subtypes have different migratory capacities irrespective of SDF1 treatment. Nevertheless, we also investigated the ability to inhibit SDF1-mediated RGC recruitment by preconditioning donor RGCs with a CXCR4 antagonist, AMD3100. Blocking CXCR4 hRGCs with 10 μM AMD3100 in our transwell assay resulted in complete inhibition of RGC recruitment by SDF1 treatment (*SI Appendix*, Fig. S4B, $42.18 \pm 10.48\%$ vs. $12.73 \pm 1.81\%$). Last, by treating hRGCs with 50 ng/mL SDF1 for three consecutive days in culture, we demonstrated that SDF1 does not affect neurite outgrowth (*SI Appendix*, Fig. S5).

Finally, we investigated the universality of SDF1-mediated RGC recruitment with RGCs derived from a different stem cell source and differentiation strategy. Human iPSCs with a constitutive green fluorescent protein (GFP) reporter were differentiated using a 2D approach (*SI Appendix*, Fig. S6 A–C) as previously described (50). Treating these GFP-RGCs with SDF1 in our transwell migration assay significantly increased RGC recruitment (SDF1: $22.22 \pm 2.31\%$; Control: $5.05 \pm 2.31\%$, *SI Appendix*, Fig. S6 D and E). While these results demonstrate that SDF1-mediated RGC recruitment is universal across cell lines and differentiation strategies, the percentage of organoid-derived RGC recruitment in response to SDF1 was greater. Therefore, despite SDF1 being able to drive neuron migration, it is critical to confirm chemokine responsiveness for different cell lines and differentiation strategies.

An SDF1 Gradient across the Neural Retina Improves the Structural Integration and Maturation of Donor RGC In Vivo. SDF1 and its receptor, CXCR4, are involved in various physiological and pathological processes, development, regeneration, and repair of the nervous system (51, 52). SDF1/CXCR4 is essential in retinal lamination, RGC and photoreceptor development (53), and axon regeneration (51). SDF1 and CXCR4 are also required for RGC survival and axon guidance in mammalian and zebrafish retinal development (54–56), and exogenous SDF1 has recently been considered for photoreceptors neuroprotection after retinal detachment (57). The role of SDF1 has also been explored for axon and optic nerve regeneration (58) but not yet explored in the transplantation setting to stimulate RGC recruitment, although CXCR4 is expressed on hESC-derived RGCs (59).

After demonstrating that SDF1 treatment enhances RGC recruitment in vitro (Fig. 2E and *SI Appendix*, Fig. S4A), we transplanted human RGCs subretinally and delivered recombinant SDF1 protein intravitreally to establish a chemokine gradient across the retina and drive donor RGC migration *in vivo* (Fig. 4A). To deliver donor RGCs, we accessed the subretinal space between the retinal pigment epithelium and photoreceptor outer segments through the sclera to avoid causing a retinotomy that could limit the effectiveness of our chemokine gradient. The lack of a retinotomy was confirmed by optical coherence tomography imminently following transplantation (*SI Appendix*, Fig. S7) or by eye during the dissection before quantification. Retinas containing a retinotomy were excluded from the migration analysis (approximately 30% of transplanted retinas). To support donor RGCs after delivery to the subretinal space and establish a proneuronal microenvironment like that of our cell culture system, we formulated our donor cells with slow-release neurotropic factors [GDNF-, BDNF-, and CNTF-loaded polyhedrin-based particles (PODs)]. Last, unlike our mouse syngeneic transplantations (Fig. 1A), retinas were collected for analysis 3 d following cell delivery to limit the immune response in our xenotransplantation experiments.

Retinal explants were prepared as flat mounts and imaged using confocal microscopy to assess donor RGC distribution (Fig. 4B). The resulting tiled, z-stacked image was reconstructed using custom semiautomated ImageJ and MATLAB scripts to identify the x-, y-, and z-position of each donor RGC within the neural retina. The z-axis position was then normalized to the thickness of each retina so those values could be superimposed and differences between experimental groups evaluated. Due to differences in each retinal

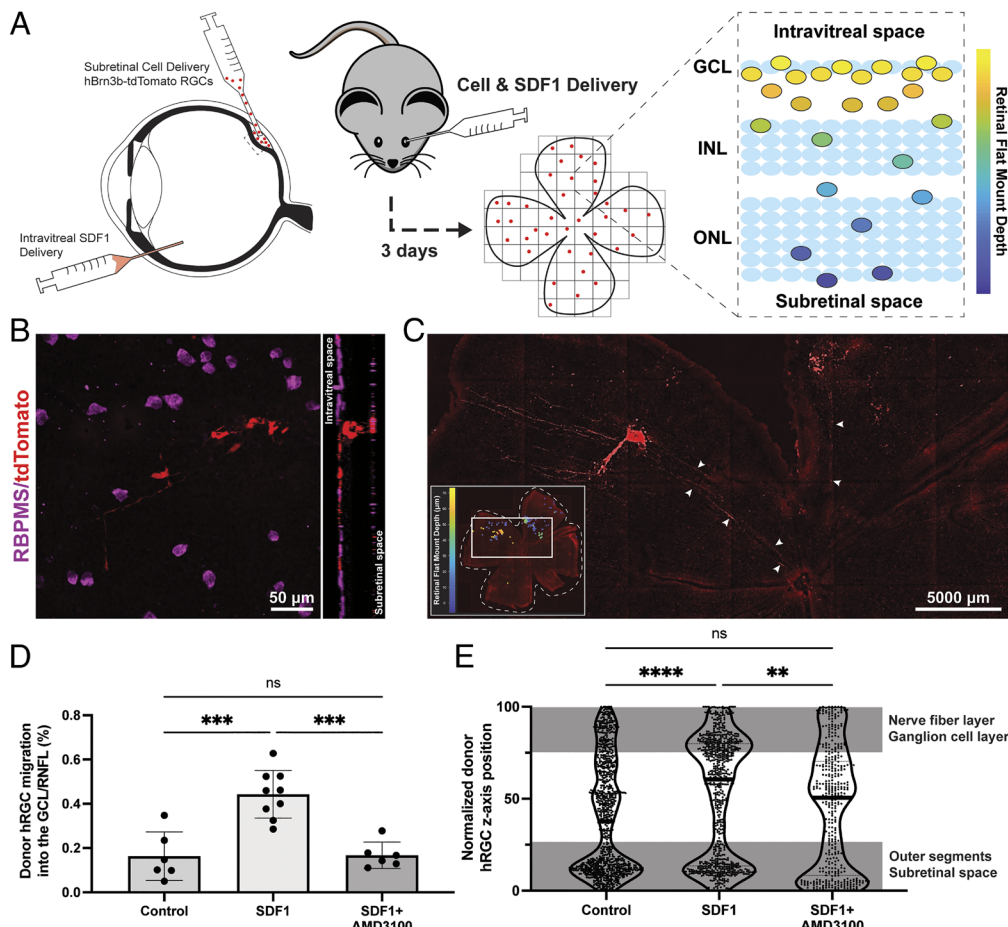


Fig. 4. Human stem cell-derived RGC xenotransplantation in mice with exogenous SDF1 gradient. (A) Schematic overview of our donor RGC and SDF1 delivery strategy to establish a chemokine gradient across the neural retina and quantification paradigm to assess structural integration of individual donor RGCs 3 d following transplantation using a 3D reconstruction of a retinal flat mount. (B) Representative en-face immunofluorescent image (max intensity projection) and orthographic projection showing donor RGC (tdTomato+, red) migration from the subretinal space toward the intravitreal space in response to SDF1 treatment. Host RGCs are shown by RBPMS+ staining (purple). (C) Representative retinal flat mount (max intensity projection) shows donor RGCs extending neurites toward the optic nerve head (white arrows) following subretinal cell delivery and intravitreal SDF1 treatment. The inlay shows a depth-coded retinal flat mount for all identified donor RGCs. (D) Quantitative analysis of donor RGC migration into the GCL/RNFL shows that the significant increase in donor RGCs translocating into the GCL/RNFL in response to SDF1 treatment is mediated through CXCR4. N = 6 to 8 mice per group. (E) Single-cell quantification of the z axis position normalized to the thickness of the retina reveals that while SDF1 treatment enhances the structural integration of donor RGCs, a significant population of donor RGCs fail to migrate and remain within the subretinal space. The nerve fiber layer and GCL were defined as the top quartile of the retina, while the subretinal space and outer segments were defined as the bottom quartile.

preparation and the difficulties defining the retinal nerve fiber layer (RNFL) from the GCL and the outer segments from the subretinal space, we defined the GCL and RNFL and the subretinal space and outer segments together as the top and bottom quartile of the retina, respectively.

Following the subretinal delivery of donor RGCs, we observed both spontaneous and chemokine-directed migration within the neural retina into the GCL/RNFL (Fig. 4*B* and *SI Appendix*, Fig. S8). Critically, because the inner limiting membrane is left intact during our transplants, this membrane could function as a stop signal, and we did not detect any cells on the vitreous surface of the retina. Moreover, we observed neurite outgrowth toward and away from the optic nerve head in a subset of transplants from those that received SDF1 (Fig. 4*C*, white arrows), likely following the topography of host RGC axons. We also confirmed that the majority of donor GFP+ RGCs and their processes express human cytoplasm protein, STEM121, suggesting that material transfer is not a significant concern for our short-term (3 d) transplantation experiments (*SI Appendix*, Fig. S9). SDF1 treatment also significantly increased RGC migration into the GCL/RNFL from $16.4 \pm 11.0\%$ to $44.3 \pm 10.8\%$ (Fig. 4*D*)—a 2.7-fold increase in migration into the GCL/RNFL. Approximately the same percentage of donor RGCs (~40%) migrated in response to SDF1 treatment in both an *in vitro* and *in vivo* environment. We do not yet know whether other intrinsic cell characteristics outside CXCR4 expression result in this similar response or whether additional SDF1 injections will further enhance RGC recruitment. The PODs formulation had no apparent effect on donor RGC soma translocation into or toward the GCL (*SI Appendix*, Fig. S10).

To better understand this response and to demonstrate a direct effect of SDF1 on donor RGCs rather than some secondary effect, we preconditioned donor RGCs with AMD3100 to block the CXCR4 receptor. Blocking SDF1 binding to the CXCR4 receptor with AMD3100 inhibited SDF1-mediated donor RGC translocation into the GCL/RNFL (Fig. 4*D*). Despite preventing migration into the GCL/RNFL, blocking CXCR4 activation with AMD3100 does not appear to completely inhibit donor RGC migration in response to SDF1, with a discrete population of donor cells in the central layers of the retina (Fig. 4*E*). Furthermore, while SDF1 treatments significantly increased the number of donor RGCs within the GCL/RNFL (Fig. 4*D*), a large population of donor RGCs failed to migrate in response to SDF1 and remained within the subretinal space (Fig. 4*E*). Staining for phosphorylated CXCR4 demonstrated that SDF1 interacts with donor and host cells in both the subretinal space and neural retina (*SI Appendix*, Fig. S11). No significant differences in total donor RGCs were detected between groups (*SI Appendix*, Fig. S12).

In a final set of transplantation experiments, we aimed to validate chemokine-directed donor cell migration across species and in different directions. To demonstrate this phenomenon, we delivered mouse stem cell-derived RGCs subretinally or intravitreally and injected SDF1 intravitreally or subretinally to establish a forward and reverse gradient across the retina, respectively (*SI Appendix*, Fig. S13 *A–C*). Two weeks after transplantation, retinas were stained for host and donor RGCs to assess donor cell integration and distribution across and within the retina with respect to the host GCL. Given the longer possible timeframes for syngeneic transplantation, donor RGC morphology was also analyzed to assess their capacity to extend their processes toward the inner plexiform layer. For both subretinal and intravitreal cell delivery, the artificial SDF1 gradient increased donor RGC migration/neurite extension in the direction of SDF1 and the percentage of donor cell processes found within the inner plexiform layer (*SI Appendix*, Fig. S13 *B–D*). Unlike our human RGCs, it was

impossible to quantitatively assess individual mouse RGCs in these transplantation experiments. Nevertheless, quantifying mouse donor RGCs at a population level further highlights that subretinal cell delivery improved RGC integration into the host retina compared to intravitreal cell delivery, irrespective of SDF1 treatment. We transplanted intact retinal organoids (*SI Appendix*, Fig. S14*A*) to the subretinal space and delivered SDF1 intravitreally to provide one final proof of concept study. Quantifying normalized donor cell distribution shows donor RGC migration/neurite extension out from the retinal organoids in the direction of our SDF1 treatment (*SI Appendix*, Fig. S14*B*).

Last, by assessing the maturation of donor RGCs after transplantation, we show that only donor RGCs that migrate into the GCL because of SDF1 treatment express mature RGC markers (Fig. 5 *A–C*). To accurately determine the number and position of donor RGCs that expressed RBPMS *in vivo*, we evaluated the colocalization of tdTomato and RBPMS in both the x-y and x-z image planes—relying on only one plane results in counting donor cells with incomplete colocalization with a bias toward those near host RGCs that express RBPMS (Fig. 5 *A* and *B*, cyan: incomplete colocalization, yellow: complete colocalization). While no RBPMS expression was observed in donor RGCs before transplantation, approximately 2% of donor RGCs identified in the GCL expressed RBPMS. Furthermore, zero cells outside the GCL expressed RBPMS (Fig. 5*C*), indicating that chemokine-directed migration itself or some molecular cue within the GCL is required to promote RGC maturation *in vivo*.

To better understand this phenomenon, we performed a pseudo-time analysis of developing RGCs (Fig. 5*D*). RGCs were classified according to their developmental state: differentiation, migration, and maturation (Fig. 5*E*). Positive regulators of migration were highest in the differentiating cells and lowest in the mature RGCs, while negative regulators of migration were the highest in mature RGCs and lowest in differentiating cells (Fig. 5*F* and *SI Appendix*, Fig. S15). These results demonstrate that RGCs must go through a migration state during normal retinal development before maturing, as defined by RBPMS expression (Fig. 5*G*). Moreover, CXCR4 expression was highest during the migration state both in terms of expression (Progenitors, 0.014; Migration, 0.094; Maturation, 0.010) and population (Progenitors, 2.2%; Migration, 24.2%; Maturation, 3.1%) (Fig. 5*G*), indicating that this receptor has an essential role during normal retinal development. Therefore, our subretinal delivery approach to RGC transplantation, in combination with directed migration, may be driving maturation by mimicking development. Nevertheless, we must still consider the possibility that molecular cues within the GCL may promote RGC maturation.

Human Retinal Neurons Primarily Migrate through the Multipolar Migration Mode following Transplantation in Mice.

To understand the mechanisms by which donor RGCs migrate through the mature retinal tissue in response to SDF1 treatment, we first investigated RGC migration patterns and kinetics *in vitro*. We confirmed the capacity for stem cell-derived RGCs to migrate via each migratory modality within 3D tissue by live cell imaging in mouse retinal organoids. Neurons migrating via somal translocation will extend a single neurite toward their final location and then pull their soma along that neurite with or without retracting it (*SI Appendix*, Fig. S16*A*). Conversely, neurons migrating via multipolar migration will extend multiple processes in different directions as they pull their soma toward their final location in a dynamic but random pattern (*SI Appendix*, Fig. S16*A*). Following translocation, RGCs lose their remaining processes and project axons toward the optic nerve. To visualize neuronal migration within retinal organoids, RGCs were differentiated using a sparse

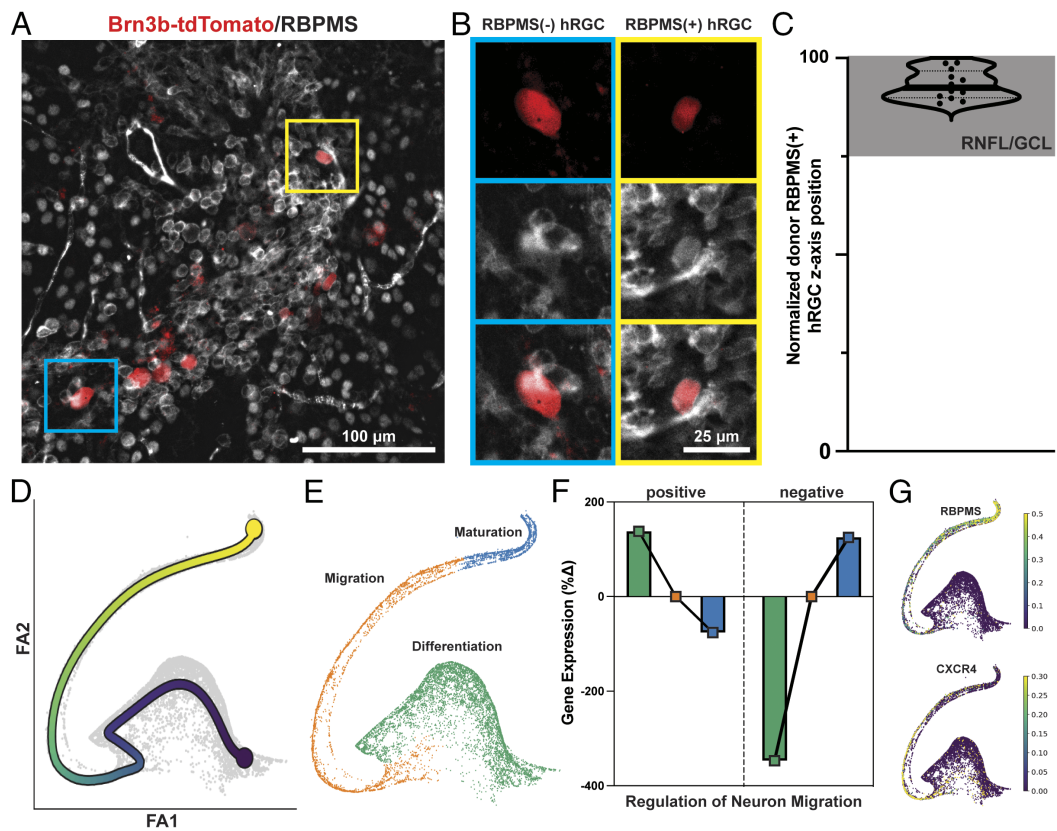


Fig. 5. In vivo maturation of human RGCs. (A) Representative immunofluorescent image of donor RGCs (red) within the GCL 3 d following transplantation in mice. RBPMS is shown in white. (B) Zoomed-in panel highlighting donor RGCs without (cyan) and with (yellow) RBPMS expression. (C) Single-cell quantification of the z axis position normalized to the thickness of the retina reveals that only donor RGC that migrate into the RNFL/GCL express RBPMS. The RNFL and GCL were defined as the top quartile of the retina. (D) Cell fate trajectory based on pseudo-time analysis of developing RGCs. (E) RGCs classified according to their developmental state in pseudo-time and expression patterns show that (F) positive regulators of migration are highest for differentiating cells and lowest for mature RGCs, while negative regulators are highest for mature RGCs and lowest for differentiating cells. (G) Feature plots of RBPMS and CXCR4 genes for RGCs show that RBPMS is expressed in mature cells and CXCR4 in migrating cells.

Thy1.2-GFP stem cell line (*SI Appendix*, Fig. S16*B*). Critically, RGCs differentiated from this reporter line express GFP within their processes, which can be observed to confirm each migratory mode. Qualitative observation of individual frames in series demonstrates that mouse stem cell-derived RGCs can migrate by somal translocation (*SI Appendix*, Fig. S16*B'* and Movie S1) and multipolar migration (*SI Appendix*, Fig. S16*B''* and Movie S1). While somal translocation was the most common migratory mode observed within the retinal organoids, these confocal traces of individual neurons represent a demonstration of spontaneous multipolar migration for mammalian stem cell-derived RGCs.

However, we could not rely on spontaneous migration to confirm these migratory modes *in vivo* because of our limited capacity to quantify live cell migration *in vivo*. Moreover, unlike mouse retinal organoids, due to the dense and robust fluorescent reporter expression within retinal organoids derived from Brn3b-tdTomato hESCs, we could not quantify migration within 3D tissues *in vitro*. Therefore, we utilized small molecule migration inhibitors to investigate the migration modes of human RGCs *in vitro* and *in vivo*. To confirm the efficacy of these inhibitor molecules and study each migration pattern, RGCs were differentiated in 3D organoid cultures, isolated by magnetic microbeads against CD90.2, and cultured on laminin-coated plates for live cell video microscopy. We temporarily destabilized the cytoskeleton of donor RGCs to alter their migratory modality between somal translocation and multipolar migration or completely inhibit cell motility. By treating RGCs with a CDK5 inhibitor (roscovitine, 15 μ M) (60, 61), multipolar migration is inhibited, and somal translocation will be the only active migratory mode (*SI Appendix*, Fig. S17*A*). Similarly, by treating RGCs with an Arp2/3 inhibitor (CK-666, 200 μ M) (62, 63), somal translocation is inhibited, and RGCs will only be capable of migration via multipolar migration (*SI Appendix*, Fig. S17*B*). RGC viability was greater than 90% for each group, indicating that each inhibitor molecule did not affect cell viability (*SI Appendix*,

*Fig. S17*C**). Each migration pattern was confirmed with an *in vitro* time-lapse study with 20-min intervals. Inhibiting somal translocation with CK666 resulted in a significant decrease in RGC migration speed and total displacement from $5.6 \pm 2.2 \mu\text{m/s}$ to $4.7 \pm 2.0 \mu\text{m/s}$ and $160.1 \pm 85.0 \mu\text{m}$ to $139.8 \pm 71.6 \mu\text{m}$, whereas inhibiting multipolar migration with roscovitine decreased their speed and total displacement to $3.2 \pm 1.5 \mu\text{m/s}$ and $93.9 \pm 54.0 \mu\text{m}$, respectively—demonstrating hESC-derived RGCs can migrate via both modalities (*SI Appendix*, Fig. S17 *D–F*). To further validate these results, we showed that the coadministration of both inhibitor molecules prevented migration in most treated cells *in vitro* (*SI Appendix*, Fig. S17 *D–F*). Somewhat surprising is that somal translocation inhibition by roscovitine treatment resulted in significantly slower RGC migration than multipolar migration inhibition by CK666 treatment, despite somal translocation being the faster migration mode. Furthermore, the average speed and displacement of cells traveling by each of the two migration modes do not sum to the average migration kinetics of the nontreated controls. This finding indicates that some off-target effects of roscovitine further limit migration or that not all RGCs have the same capacity to migrate by each mode. The discrete cell populations observed in the violin plots suggest the latter explanation is more likely (*SI Appendix*, Fig. S17 *D* and *E*) while also demonstrating the effectiveness of each small molecule in inhibiting each mode of migration independently.

By applying these same inhibitor molecules to our *in vivo* transplantation paradigm, we demonstrated distinct patterns of donor RGC coverage and positioning within the neural retina (Fig. 6 *A–D*). Our results show that impairing somal translocation by CK666 preconditioning does not affect the percentage of donor RGCs that migrate into the GCL/RNFL in response to SDF1 (No inhibition: $44.3 \pm 10.8\%$; somal translocation inhibition: $47.2 \pm 12.0\%$, Fig. 6*E*). However, inhibition of multipolar migration by roscovitine preconditioning significantly limits the percentage of donor RGCs that migrate into the GCL/RNFL in

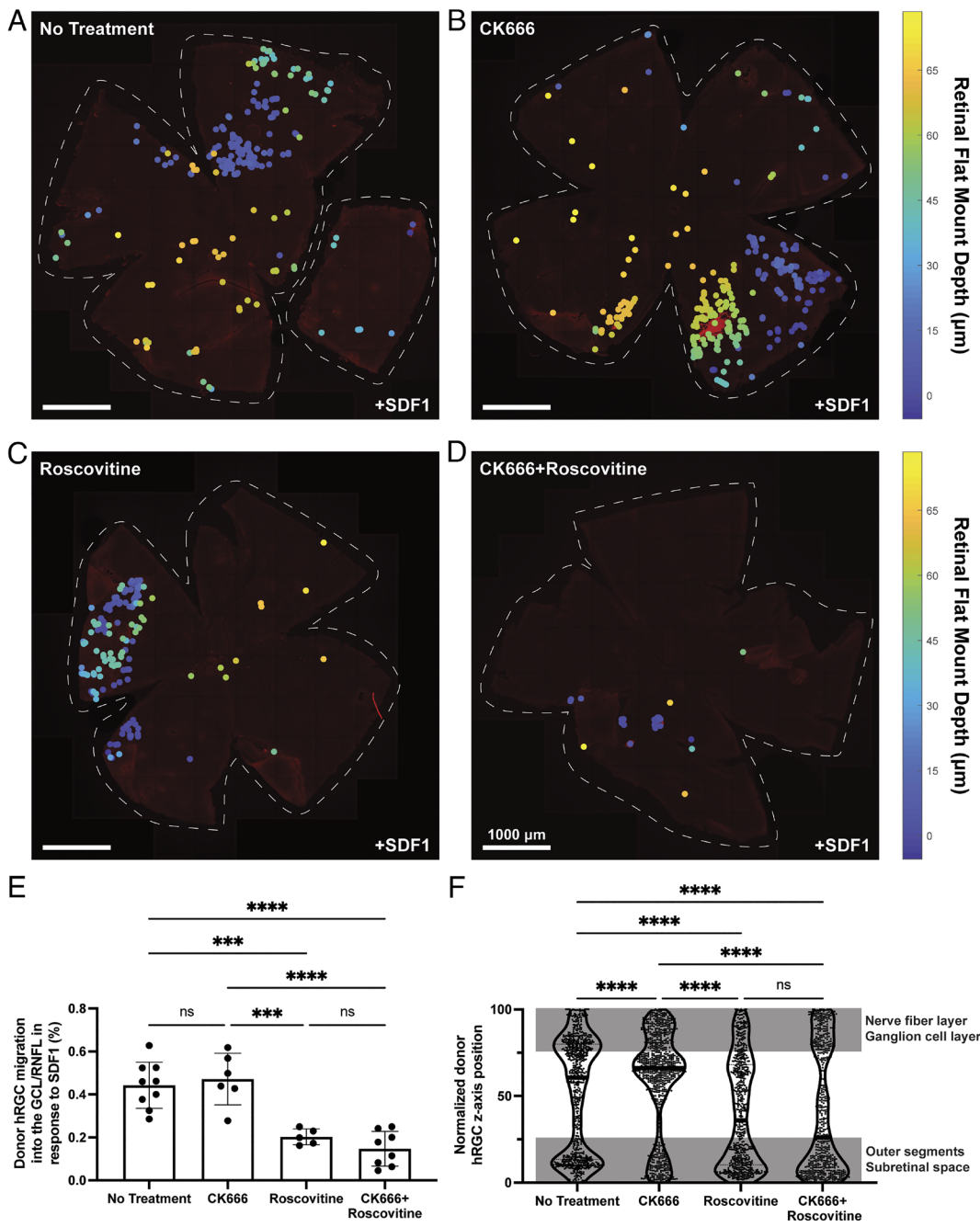


Fig. 6. Distinct patterns of donor neuron translocation following SDF1 treatment in mice. (A) Representative depth-coded color map overlaid on retinas transplanted with donor RGCs preconditioned with DMSO (no treatment control), (B) CK666, an ST inhibitor, (C) roscovitine, an MP migration inhibitor, and (D) CK666 + roscovitine to modulate their migratory modality shows donor RGC distribution and coverage across and within the retina following SDF1 treatment. Deep blue represents the subretinal space, while yellow represents the GCL/RNFL. (E) Quantitative analysis of donor RGC migration into the GCL/RNFL in response to SDF1 shows no difference between control donor RGC and those preconditioned with CK666, but a significant decrease in translocation for donor RGC treated with roscovitine and CK666 + roscovitine, indicating MP migration, but not ST, is required for donor RGCs to migrate into the GCL/RNFL through the neural retina. $N = 5$ to 8 mice per group. (F) Single-cell quantification of the z-axis position normalized to the thickness of the retina reveals that while there was no significant difference in the number of donor RGC structurally integrating into the GCL/RNFL between the control donor RGCs and those preconditioned with CK666, CK666 preconditioning resulted in a significant increase in overall migration toward the GCL/RNFL. The nerve fiber layer and GCL were defined as the top quartile of the retina, while the subretinal space and outer segments were defined as the bottom quartile.

response to SDF1 compared to the CK666 preconditioning and no treatment groups (multipolar migration inhibition: $20 \pm 3.7\%$, Fig. 6E). Critically, each mode of neural migration inhibition did not affect the total number of surviving donor RGCs (*SI Appendix*, Fig. S12). The fact that there were no significant differences between dual inhibition of migratory modes and multipolar migration inhibition alone (dual inhibition: $14.7 \pm 8.1\%$, Fig. 6E) indicates that multipolar migration is the primary mode by which donor RGCs migrate within the neural retina in response to SDF1 treatment. Despite no significant difference in the number of donor RGCs structurally integrating into the GCL/RNFL following SDF1 treatment between the control donor RGCs and those preconditioned with CK666, CK666 preconditioning resulted in a significant increase in overall migration toward the GCL/RNFL (Fig. 6F). However, while CK666 preconditioning increased the overall migration toward the GCL/RNFL, we do not yet know why these donor RGCs failed to continue into the GCL/RNFL.

RGCs can also migrate tangentially during development and age-related degeneration as a part of retinal refinement (64, 65), yet we see limited migration in the *x*- and *y*-axes following transplantation. Unfortunately, SDF1 treatments alone were insufficient to significantly increase donor RGC retinal coverage, defined as the percentage of tiles per retina with one or more donor RGCs (*SI Appendix*, Fig. S18). However, in combination with somal translocation inhibition by CK666 preconditioning, donor RGC retinal coverage was significantly increased from $23.6 \pm 7.8\%$ for donor RGCs without preconditioning, and no SDF1 injections to $50.5 \pm 27.5\%$ for donor RGCs preconditioned with CK666 and SDF1 injections (*SI Appendix*, Fig. S18).

SDF1 Treatment Causes the Displacement of Endogenously Regenerated Retinal Neurons In Situ. Despite our CXCR4 blocking experiment demonstrating the direct effect of SDF1 on donor RGC translocation into the GCL, host neurons within

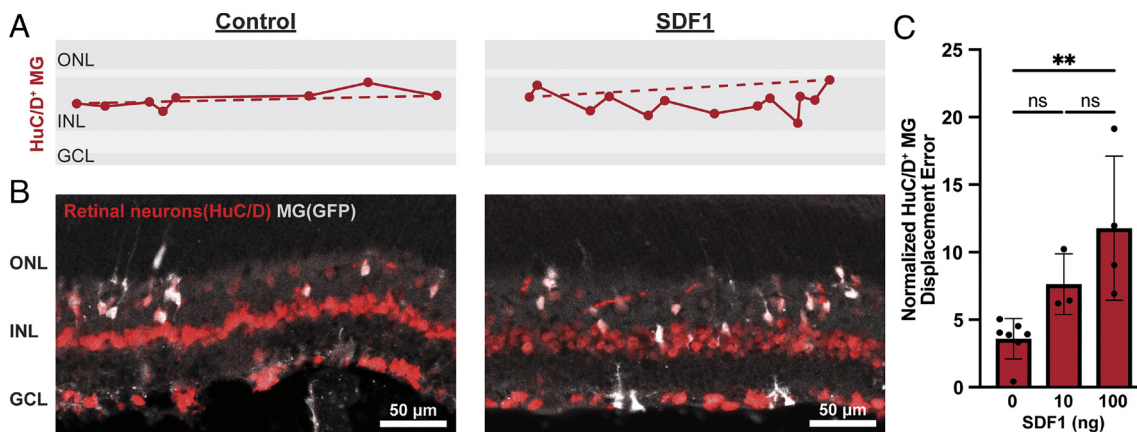


Fig. 7. Endogenous reprogrammed neurons respond to SDF1 treatment in the retina. (A) Representative quantitative assessment of NDE showing the positions of HuC/D positive MGs (red and white colocalization) and (B) immunofluorescent images of retinal sections stained for MGs (GFP positive, pseudo-colored gray) and retinal neurons (HuC/D positive, red) with and without SDF1 treatments. (C) Quantification of NDE for HuC/D positive MGs in an NMDA-damaged model at 0, 10, and 100 ng SDF1 shows a dose-dependent response. GCL, ganglion cell layer; INL, inner nuclear layer; ONL, outer nuclear layer.

the retina also express CXCR4 (66) and could be adversely affected by SDF1. To investigate the effects of SDF1 on retinal lamination and position of host retinal neurons, we delivered a range of concentrations (0, 1, 10, and 200 ng SDF1) into the mouse vitreous and collected retinas for histology 24 h after the injection. Hematoxylin and eosin stained sections of the neural retina following intravitreal injection SDF1 showed no apparent changes in retinal lamination (*SI Appendix*, Fig. S19*A*). Retinal sections were also stained for host neurons and glia (RGCs, bipolar cells, photoreceptors, and Müller glia) to visualize any effects of SDF1 treatments. We observed no differences in RGC, bipolar cell, and photoreceptor morphology and position between sections and concentrations of SDF1 (*SI Appendix*, Fig. S19 *B–D*), but Müller glia appeared to be reacting to SDF1 treatments (*SI Appendix*, Fig. S19*E*). To quantify this reaction, we calculated the normalized displacement error (NDE), defined as the difference between the total segment length connecting each point and a straight line normalized to the total number of points (*SI Appendix*, Fig. S20). For example, a high NDE will be associated with increased total displacement from the mean. By applying this analysis, we demonstrated that Müller glia will have increased displacement with increasing concentrations of SDF1 (*SI Appendix*, Fig. S19*F*).

While stem cell replacement therapies represent one approach to restoring retinal neurons lost in glaucoma and other optic neuropathies, stimulating neurogenesis in the retina through endogenous reprogramming of Müller glia may be an alternative regenerative strategy. Todd et al. demonstrated efficient stimulation of retinal regeneration from Müller glia in adult mice using a combination of proneuronal transcription factors; however, following neurogenesis, RGC-like neurons mostly fail to migrate to the GCL (11). Here, we sought to improve the migration of Müller glia-derived newborn neurons using SDF1 to demonstrate the universality of chemokine-directed migration for regenerative medicine.

Müller glia were reprogrammed into RGC-like neurons as previously described (11). Approximately 1 wk after initiating reprogramming, host RGCs were ablated to mimic the loss of RGCs in glaucoma using NMDA-induced toxicity. After a short recovery period (1 to 2 d), SDF1 was injected intravitreally to test whether endogenously regenerated neurons can be recruited by SDF1. Two weeks following SDF1 treatment, the locations of Müller glia-derived neurons (GFP+/HuC/D+) were quantified (Fig. 7 *A* and *B*). We found that SDF1 elicited a dose-dependent displacement of Müller glia-derived neurons. Newly generated neurons showed a NDE from 3.59 ± 1.50 to 11.8 ± 5.33 at 0 and 100 ng SDF1

delivery, respectively (Fig. 7*C*)—a 3.3-fold increase in displacement. These results highlight the potential to direct reprogrammed neuron migration *in situ* with chemokines. In addition to regenerative medicine, repositioning Müller glia-derived neurons *in vivo* may also enable improved access for quantitative assessment, such as whole-cell patch-clamp recordings. However, we do not yet know the ideal timing for SDF1 treatment nor whether displacement occurs before or after reprogramming. The delivery of a slow-release formation of SDF1 may help to solve this problem in the future and lead to enhanced neural recruitment for both endogenously reprogrammed and stem cell-derived donor neurons.

Alternatively, other chemokines may be better suited to direct newborn neuron migration. By applying a similar *in silico* approach to what we previously described (*SI Appendix*, Fig. S21*A*), we can identify additional targets and the optimal treatment timing to improve the structural integration of Müller glia-derived neurons by manipulating the retinal microenvironment with chemokines. Like donor RGCs, Müller glia-derived RGCs express genes associated with multipolar migration and somal translocation (*SI Appendix*, Fig. S21*B*), suggesting the possibility of controlling their migratory profile to improve integration. Unsurprisingly, these newborn neurons have greater expression of migratory genes shortly after Müller glia reprogramming, with multipolar migration genes remaining up-regulated at later time points (3 vs. 8 wk) while somal translocation genes are reduced (*SI Appendix*, Fig. S21*B*). Unlike host and stem cell-derived RGCs, Müller glia-derived neurons express a different profile of chemokine receptors (*SI Appendix*, Fig. S21*C*). While our intravitreally SDF1 treatment resulted in the displacement from the inner nuclear layer, CXCR4 expression in these cells is at its highest level 8 wk post-reprogramming, indicating a later SDF1 treatment may be more beneficial. Nevertheless, these *in silico* results suggest that while a later SDF1 treatment may better modulate Müller glia-derived neuron migration, there are several receptors with higher expression, such as Robo2, Ptprz1, and Ntrk2 (*SI Appendix*, Fig. S21*C*), that could be used in the future to enhance neural recruitment of endogenously regenerated neurons.

Conclusions

The transplantation of stem cell-derived dopaminergic neurons, motor neurons, photoreceptors, retinal pigment epithelium, mesenchymal stem cells, and other cell types has reached the stage of clinical trials. The preclinical studies of cell engraftment into

various animal models highlighted the importance of the niche and the need to better control cell behavior after delivery by engineering cell-intrinsic and extrinsic factors. Here, we describe the framework to identify microenvironment cues to control a specific donor cell behavior using RGCs in the eye as a substrate and migration as a function of interest. This “*in silico*–*in vitro*–*in vivo*” funnel can be applied to other cellular processes, including synapse formation, phagocytosis, insulin production, axon growth, etc.

Moreover, identifying SDF1 as a chemokine, leading to a greater than twofold increase in donor cell migration, allowed us to study the migration of neurons in the controlled and accessible ecosystem of the eye. We have demonstrated that RGCs can migrate via somal translocation and multipolar migration modes *in vitro*; however, they primarily use multipolar migration *in vivo* in the adult retina to navigate the developed tissue architecture. Donor RGC migration allows us to direct donor cells within the GCL within the first few days after transplantation and promote maturation, allowing them to integrate into existing retinal circuitry.

Methods

RGC Differentiation and Isolation. RGCs were differentiated from either Thy1-GFP mouse iPSC (C57Bl/6 background) or H9-BRN3B:tdTomatoThy1.2-hESCs in 3D retinal organoid cultures as previously described (13, 30, 31). Mature mouse and human retinal organoids were dissociated and then isolated by magnetic microbead sorting for Thy1.2+ cells.

Single-cell RNA Sequencing Data Analysis. Single-cell RNA sequencing data analysis was performed using the datasets obtained from Wang et al. for the human adult retina (34) and Sridhar et al. for fetal (FD59, FD82, and FD105) and hPSC-derived retinal organoids (OD45 and OD60) (33). We used Python- and R-based dependencies to process the data by utilizing the packages for the main [Seurat (67) and scanpy (68)], gene set enrichment analysis [escape (69)], and pseudo-time/cell fates [scFates (70)] analyses. A full description of the pipeline is available in *SI Appendix* and available on GitHub at <https://github.com/mcrewcow/BaranovLab>.

In Vitro Cell Recruitment Assay. The effects of a panel of chemokines and a CXCR4 antagonist on cell recruitment *in vitro* were investigated using porous membrane cell culture inserts. The upper compartment was seeded with 1×10^5 hRGCs, and each chemokine was added to the bottom compartment: 50 ng/mL aFGF, 100 ng/mL Netrin, 500 ng/mL SHH, 1,000 ng/mL Slit, and 10, 50, 200, and 500 ng/mL SDF1. After 24 h, the RGCs were fixed and imaged on an Olympus IX83-FV3000 confocal microscope. RGC recruitment was reported as the ratio of RGCs on the basal surface of the membrane to the total number of RGCs.

Donor Cell Transplantation. All transplantation studies were approved by the Schepens Eye Research Institute of Mass. Eye and Ear Institution Animal Care and Use Committee (IACUC) following the Association for Research in Vision and Ophthalmology (ARVO) guidelines. After cell isolation, RGCs were formulated in RGC media at 1 to 5×10^5 cells/mL. The RGC suspension was then kept on ice for 1 to 2 h to allow damaged cell membranes to seal and enable time to precondition donor cells with small molecules before transplantation. For the loss-of-function studies, RGCs were preconditioned with 10 μM AMD3100, a CXCR4 antagonist, 200 μM CK666 (Sigma, SML0006), a somal translocation inhibitor, and/or 15 μM roscovitine (Enzo Life Sciences, ALX-380-033), a multipolar migration inhibitor for 1 h on ice. Excess small molecule inhibitors were subsequently removed by centrifugation. After membrane recovery and preconditioning, donor RGCs were formulated for transplantation at 2×10^4 viable cells/ μL in RGC media containing slow-release neurotropic factors (150 U/ μL GDNF-, BDNF-, and CNTF-loaded PODs; Cell Guidance Systems, PPH1, PPH2, and PPH59) to support cell survival *in vivo*.

Intravitreal and subretinal injections were performed in young adult mice (1- to 4-mo-old) under a general (ketamine/xylazine intraperitoneal injections) and local (0.5% proparacaine eye drops) anesthetic. The donor RGC suspension (1 μL) was delivered intravitreally or subretinally through a beveled glass microneedle (80 μm inner diameter) at a 1 $\mu\text{L}/\text{min}$ flow rate. Imminently following donor

cell delivery, 10 ng SDF1 (1 μL) was delivered on the reverse side of the retina (subretinal cells–intravitreal SDF1 or intravitreal cells–subretinal SDF1) to establish a chemokine gradient across the neural retina. The subretinal space was accessed through the sclera to deliver cells or SDF1 between the retinal pigment epithelium and photoreceptor outer segments. Mice were maintained on a standard 12-h day–night cycle and euthanized at each experimental endpoint (2 wk for syngeneic transplantation and 3 d for xenotransplantation) by CO₂ inhalation. To access the transplantation outcome and donor RGC structural integration, eyes were imminently enucleated, fixed for 24 h at room temperature in 4% paraformaldehyde, and then processed for retinal flat-mount preparation.

The position of donor RGCs within the host retina was quantified using custom ImageJ and MATLAB scripts. The number and position (x, y, z) of donor RGCs were quantified using the 3D object counter plugin, and the GCL was identified as the z -plane containing RBMPS+ host cells. These data were used to calculate the percentage of donor RGCs that migrated into the GCL. To compare z -positions of donor RGCs across retinas, the z -position was normalized between 0 and 100 using min/max scaling. Donor RGC coverage was calculated as the percentage of tiles per retina with one or more donor RGC.

Endogenous Reprogramming. All endogenous reprogramming studies were approved by the University of Washington IACUC following the ARVO guidelines. Müller glia were reprogrammed into RGCs as previously described (11). Glast-CreER:LNL-tTA:tetO-mAscl1-GFP-tetO:Atoh1 adult mice were used to specifically induce Ascl1:Atoh1 in Müller glia. Male and female mice were used in all experiments. Tamoxifen (1.5 mg per 100 mL of corn oil) was injected intraperitoneally in adult mice for 5 consecutive days to induce endogenous reprogramming. Approximately 1 wk later, 100 μM NMDA (1.5 μL) was injected intravitreally with a 32-gauge Hamilton syringe to cause host RGC death. For induced migration experiments, 0, 10, or 100 ng SDF1 was injected intravitreally 2 d following the NMDA damage, and the eyes were enucleated 2 wk later for analysis. For single-cell RNA sequencing studies, animals were euthanized according to the University of Washington Institutional Animal Care and Use Committee guidelines, and retinas were collected 8 wk post-reprogramming without exogenous SDF1 treatment.

Statistical Analysis. Statistical significance was calculated using GraphPad PRISM 9 using an unpaired *t* test or a Tukey one-way ANOVA. Error bars represent the mean \pm SD of measurements (* $P < 0.05$, ** $P < 0.01$, *** $P < 0.001$, and **** $P < 0.0001$). Each dot within a bar plot represents an individual retina or well, while each dot with a violin plot represents an individual cell.

Detailed Methods Description. A detailed description of the methods used to produce the results in this work is available in *SI Appendix*.

Data, Materials, and Software Availability. The raw single-cell RNA sequencing data of human fetal retinas and organoids from ref. 33, human adult retina from ref. 34, and reprogrammed Müller glia (3 wk post-reprogramming) from ref. 11 used in this study are available in the Gene Expression Omnibus (GEO) database under accession codes [GSE142526](https://www.ncbi.nlm.nih.gov/geo/query/acc.cgi?acc=GSE142526), [GSE196235](https://www.ncbi.nlm.nih.gov/geo/query/acc.cgi?acc=GSE196235), and [GSE184286](https://www.ncbi.nlm.nih.gov/geo/query/acc.cgi?acc=GSE184286). The single-cell data can be visualized in the Broad Institute’s Single Cell Portal at https://singlecell.broadinstitute.org/single_cell/study/SCP2324 and https://singlecell.broadinstitute.org/single_cell/study/SCP2328. These include the integrated and individually processed human fetal retina, human adult retina, and mouse Müller glia (3 and 8 wk) datasets, respectively. The processed RNA sequencing data generated in this study are available on GitHub at <https://github.com/mcrewcow/BaranovLab>.

ACKNOWLEDGMENTS. We would like to thank Connor Finkbeiner for their advice in processing the raw single-cell RNA sequencing fetal and organoid data, Joshua Sanes for Thy1-GFP mice, Donald Zack for providing the Brn3b-tdTomato hESCs, and Randy Huang for flow cytometry support. NIH/NEI-F32EY033211 (J.R.S.), NIH/NEI-L70EY034355 (J.R.S.), NIH/NEI-T32EY007145 (MBED fellowship, J.R.S.), NIH/NEI-K99EY033402 (L.T.), NIH/NEI-5U24EY029893-03 (P.B.), NIH/NEI-P30EY003790 (Core Facility Grant), Bright Focus Foundation-G2020231 (P.B.), NIH/NEI RO1EY021482 (T.A.R.), Gilbert Family Foundation-GFF00 (P.B. and T.A.R.)

Author affiliations: ^aThe Schepens Eye Research Institute of Massachusetts Eye and Ear, Boston, MA 02114; ^bDepartment of Ophthalmology, Harvard Medical School, Boston, MA 02114; and ^cDepartment of Biological Structure, University of Washington, Seattle, WA 98195

1. V.I. Collaborators *et al.*, Causes of blindness and vision impairment in 2020 and trends over 30 years, and prevalence of avoidable blindness in relation to VISION 2020: The right to sight: An analysis for the Global Burden of Disease Study. *Lancet Glob. Health* **9**, e144–e160 (2020). 10.1016/s2214-109x(20)30489-7.
2. Y.-C. Tham *et al.*, Global prevalence of glaucoma and projections of glaucoma burden through 2040: A systematic review and meta-analysis. *Ophthalmology* **121**, 2081–2090 (2014).
3. T. Z. Khatib, K. R. Martin, Neuroprotection in glaucoma: Towards clinical trials and precision medicine. *Curr. Eye Res.* **45**, 327–338 (2019).
4. M. Almasieh, L. A. Levin, Neuroprotection in glaucoma: Animal models and clinical trials. *Annu. Rev. Vis. Sci.* **3**, 1–30 (2016).
5. J. F. Martin, R. A. Poché, Awakening the regenerative potential of the mammalian retina. *Development* **146**, dev182642 (2019).
6. J. Hertz, J. L. Goldberg, Retinal ganglion cell transplantation: Survival and integration. *Invest. Ophthalmol. Visual Sci.* **48**, 5092–5092 (2007).
7. J. Hertz *et al.*, Survival and integration of developing and progenitor-derived retinal ganglion cells following transplantation. *Cell Transf.* **23**, 855–872 (2014).
8. P. Venugopalan *et al.*, Transplanted neurons integrate into adult retinas and respond to light. *Nat. Commun.* **7**, 10472 (2016).
9. M. Eiraku *et al.*, Self-organizing optic-cup morphogenesis in three-dimensional culture. *Nature* **472**, 51–56 (2011).
10. M. Eiraku, Y. Sasai, Mouse embryonic stem cell culture for generation of three-dimensional retinal and cortical tissues. *Nat. Protoc.* **7**, 69–79 (2012).
11. L. Todd *et al.*, Efficient stimulation of retinal regeneration from Müller glia in adult mice using combinations of proneural bHLH transcription factors. *Cell Rep.* **37**, 109857 (2021).
12. L. I. Benowitz, Z. He, J. L. Goldberg, Reaching the brain: Advances in optic nerve regeneration. *Exp. Neurol.* **287**, 365–373 (2017).
13. J. Oswald, E. Kegeles, T. Minelli, P. Volchkov, P. Baranov, Transplantation of miPSC/mESC-derived retinal ganglion cells into healthy and glaucomatous retinas. *Mol. Ther. Methods Clin. Dev.* **21**, 180–198 (2021).
14. T. Perepelkina, E. Kegeles, P. Baranov, Optimizing the conditions and use of synthetic matrix for three-dimensional in vitro retinal differentiation from mouse pluripotent cells. *Tissue Eng. Part C Methods* **25**, 433–445 (2019).
15. E. Kegeles, T. Perepelkina, P. Baranov, Semi-automated approach for retinal tissue differentiation. *Transl. Vis. Sci. Technol.* **9**, 24–24 (2020).
16. E. Kegeles, A. Naumov, E. A. Karpulevich, P. Volchkov, P. Baranov, Convolutional neural networks can predict retinal differentiation in retinal organoids. *Front. Cell Neurosci.* **14**, 171 (2020).
17. C. Pedler, The inner limiting membrane of the retina. *Br. J. Ophthalmol.* **45**, 423–438 (1961).
18. M. Hoon, H. Okawa, L. D. Santina, R. O. L. Wong, Functional architecture of the retina: Development and disease. *Prog. Retin. Eye Res.* **42**, 44–84 (2014).
19. S. Grade, M. Götz, Neuronal replacement therapy: Previous achievements and challenges ahead. *Npj Regen. Med.* **2**, 29 (2017).
20. K. Y. Zhang *et al.*, Role of the internal limiting membrane in structural engraftment and topographic spacing of transplanted human stem cell-derived retinal ganglion cells. *Stem Cell Rep.* **16**, 149–167 (2021).
21. E. A. Aguzzi *et al.*, Internal limiting membrane disruption facilitates engraftment of transplanted human stem cell derived retinal ganglion cells. *biorxiv* [Preprint] (2022). <https://doi.org/10.1101/2022.12.13.519327> (Accessed 13 December 2022).
22. R. Gelman, W. Stevenson, C. Ponce, D. Agarwal, J. B. Christoforidis, Retinal damage induced by internal limiting membrane removal. *J. Ophthalmol.* **2015**, 939748 (2015).
23. F. J. Livesey, C. L. Cepko, Vertebrate neural cell-fate determination: Lessons from the retina. *Nat. Rev. Neurosci.* **2**, 109–118 (2001).
24. A. Hoshino *et al.*, Molecular anatomy of the developing human retina. *Dev. Cell* **43**, 763–779.e4 (2017).
25. C. L. Cepko, C. P. Austin, X. Yang, M. Alexiades, D. Ezzeddine, Cell fate determination in the vertebrate retina. *Proc. Natl. Acad. Sci. U.S.A.* **93**, 589–595 (1996).
26. J. N. Kay, Radial migration: Retinal neurons hold on for the ride. *J. Cell Biol.* **215**, 147–149 (2016).
27. K. Hayashi, K. Kubo, A. Kitazawa, K. Nakajima, Cellular dynamics of neuronal migration in the hippocampus. *Front. Neurosci-swit* **9**, 135 (2015).
28. I.Y. Buchsbaum, S. Cappello, Neuronal migration in the CNS during development and disease: Insights from *in vivo* and *in vitro* models. *Development* **146**, dev163766 (2019).
29. E. Kokovay *et al.*, Adult SVZ lineage cells home to and leave the vascular niche via differential responses to SDF1/CXCR4 signaling. *Cell Stem Cell* **7**, 163–173 (2010).
30. K. J. Wahlin *et al.*, CRISPR generated SIX6 and POU4F2 reporters allow identification of brain and optic transcriptional differences in human PSC-derived organoids. *Front. Cell Dev. Biol.* **9**, 764725 (2021).
31. C. M. Fligor, K.-C. Huang, S. S. Lavekar, K. B. VanderWall, J. S. Meyer, Differentiation of retinal organoids from human pluripotent stem cells. *Methods Cell Biol.* **159**, 279–302 (2020).
32. M. M. Riccomagno *et al.*, Cas adaptor proteins organize the retinal ganglion cell layer downstream of integrin signaling. *Neuron* **81**, 779–786 (2014).
33. A. Sripathi *et al.*, Single-cell transcriptomic comparison of human fetal retina, hPSC-derived retinal organoids, and long-term retinal cultures. *Cell Rep.* **30**, 1644–1659.e4 (2020).
34. S. K. Wang *et al.*, Single-cell multilane of the human retina and deep learning nominate causal variants in complex eye diseases. *Cell Genom* **2**, 100164 (2022).
35. I. Evsyukova, C. Plestant, E. S. Anton, Integrative mechanisms of oriented neuronal migration in the developing brain. *Annu. Rev. Cell Dev. Biol.* **29**, 299–353 (2013).
36. R. Amini, M. Rocha-Martins, C. Norden, Neuronal migration and lamination in the vertebrate retina. *Front. Neurosci.* **11**, 742 (2017).
37. F. R. Zolessi, L. Poggi, C. J. Wilkinson, C.-B. Chien, W. A. Harris, Polarization and orientation of retinal ganglion cells in vivo. *Neural Dev.* **1**, 2 (2006).
38. B. Nadarajah, J. E. Brunstrom, J. Grutzendler, R. O. L. Wong, A. L. Pearlman, Two modes of radial migration in early development of the cerebral cortex. *Nat. Neurosci.* **4**, 143–150 (2001).
39. J. Ichá, C. Kunath, M. Rocha-Martins, C. Norden, Independent modes of ganglion cell translocation ensure correct lamination of the zebrafish retina. *J. Cell Biol.* **215**, 259–275 (2016).
40. I. Soto *et al.*, Retinal ganglion cells downregulate gene expression and lose their axons within the optic nerve head in a mouse glaucoma model. *J. Neurosci.* **28**, 548–561 (2008).
41. N. M. Tran *et al.*, Single-cell profiles of retinal ganglion cells differing in resilience to injury reveal neuroprotective genes. *Neuron* **104**, 1039–1055.e12 (2019).
42. N. Borchering, J. Andrews, escape: Easy single cell analysis platform for enrichment (R package, Version 1.5.1, 2022).
43. N. Borchering *et al.*, Mapping the immune environment in clear cell renal carcinoma by single-cell genomics. *Commun. Biol.* **4**, 122 (2021).
44. R. Amini, M. Rocha-Martins, C. Norden, Neuronal migration and lamination in the vertebrate retina. *Front. Neurosci-swit* **11**, 742 (2018).
45. K.-Y. Huang, H.-H. Lin, The activation and signaling mechanisms of GPR56/ADGRG1 in melanoma cell. *Front. Oncol.* **8**, 304 (2018).
46. C.-A. Chen *et al.*, The expanding clinical phenotype of Bosch-Boonstra-Schaaf optic atrophy syndrome: 20 new cases and possible genotype–phenotype correlations. *Genet. Med.* **18**, 1143–1150 (2016).
47. J.-R. Martinez-Morales *et al.*, Differentiation of the vertebrate retina is coordinated by an FGF signaling center. *Dev. Cell* **8**, 565–574 (2005).
48. K. L. McCabe, E. C. Gunther, T. A. Reh, The development of the pattern of retinal ganglion cells in the chick retina: Mechanisms that control differentiation. *Dev. Camb. Engl.* **126**, 5713–5724 (1999).
49. Y. P. Wang *et al.*, Development of normal retinal organization depends on Sonic hedgehog signaling from ganglion cells. *Nat. Neurosci.* **5**, 831–832 (2002).
50. V. M. Sluch *et al.*, Enhanced stem cell differentiation and immunopurification of genome engineered human retinal ganglion cells. *Stem Cell Transl. Med.* **6**, 1972–1986 (2017).
51. L. Xie *et al.*, Monocyte-derived SDF1 supports optic nerve regeneration and alters retinal ganglion cells' response to Pten deletion. *Proc. Natl. Acad. Sci. U.S.A.* **119**, e2113751119 (2022).
52. Y. Zhu, T. Matsumoto, S. Mikami, T. Nagasawa, F. Murakami, SDF1/CXCR4 signalling regulates two distinct processes of cerebellar neuronal migration and its depletion leads to abnormal pontine nuclei formation. *Development* **136**, 1919–1928 (2009).
53. J. Shimizu *et al.*, Interaction between SDF1 and CXCR4 promotes photoreceptor differentiation via upregulation of NF-κB pathway signaling activity in Pax6 gene-transfected photoreceptor precursors. *Ophthalmic Res.* **63**, 392–403 (2020).
54. S. H. Chalasani *et al.*, Stromal cell-derived factor-1 antagonizes slit/robo signaling in vivo. *J. Neurosci.* **27**, 973–980 (2007).
55. S. H. Chalasani *et al.*, The chemokine stromal cell-derived factor-1 promotes the survival of embryonic retinal ganglion cells. *J. Neurosci.* **23**, 4601–4612 (2003).
56. Q. Li *et al.*, Chemokine signaling guides axons within the retina in zebrafish. *J. Neurosci.* **25**, 1711–1717 (2005).
57. H. Otsuka *et al.*, Stromal cell-derived factor-1 is essential for photoreceptor cell protection in retinal detachment. *Am. J. Pathol.* **177**, 2268–2277 (2010).
58. A. Heskamp *et al.*, CXCL12/SDF-1 facilitates optic nerve regeneration. *Neurobiol. Dis.* **55**, 76–86 (2013).
59. J. G. Aparicio *et al.*, Temporal expression of CD184(CXCR4) and CD171(L1CAM) identifies distinct early developmental stages of human retinal ganglion cells in embryonic stem cell derived retina. *Exp. Eye Res.* **154**, 177–189 (2017).
60. B. Menn *et al.*, Delayed treatment with systemic (S)-rescovitinide provides neuroprotection and inhibits *in vivo* CDK5 activity increase in animal stroke models. *PLoS One* **5**, e12117 (2010).
61. G. Mushtaq *et al.*, Neuroprotective mechanisms mediated by CDK5 inhibition. *Curr. Pharm. Design* **22**, 527–534 (2016).
62. B. Hetrick, M. S. Han, L. A. Helgeson, B. J. Nolen, Small molecules CK-666 and CK-869 inhibit actin-related protein 2/3 complex by blocking an activating conformational change. *Chem. Biol.* **20**, 701–712 (2013).
63. J. H. Henson *et al.*, Arp2/3 complex inhibition radically alters lamellipodial actin architecture, suspended cell shape, and the cell spreading process. *Mol. Biol. Cell* **26**, 887–900 (2015).
64. P. M. J. Quinn, J. Wijnholds, Retinogenesis of the human fetal retina: An apical polarity perspective. *Genes Basel* **10**, 987 (2019).
65. B. E. Reese, L. Galli-Resta, The role of tangential dispersion in retinal mosaic formation. *Prog. Retin. Eye Res.* **21**, 153–168 (2002).
66. T. Liu, X. Tang, L. Yao, H. Song, Expression and significance of SDF-1 and its receptor CXCR4 in the retina of pregnant rats after optic nerve injury. *Eur. J. Inflamm.* **16**, 2058739218819675 (2018).
67. R. Satija, J. A. Farrell, D. Gennert, A. F. Schier, A. Regev, Spatial reconstruction of single-cell gene expression data. *Nat. Biotechnol.* **33**, 495–502 (2015).
68. F. A. Wolf, P. Angerer, F. J. Theis, SCANPY: Large-scale single-cell gene expression data analysis. *Genome Biol.* **19**, 15 (2018).
69. D. A. Baribe *et al.*, Systematic RNA interference reveals that oncogenic KRAS-driven cancers require TBK1. *Nature* **462**, 108–112 (2009).
70. L. Faure, R. Soldatov, P. V. Kharchenko, I. Adamleyko, scFates: A scalable python package for advanced pseudotime and bifurcation analysis from single-cell data. *Bioinformatics* **39**, btac746 (2022).